

Recent Advancements in Doped Titanium Dioxide (TiO₂) Nanostructures for Photocatalytic Dye Degradation

N. A. Narewadikar^a and K. Y. Rajpure^{a,*}

^a Electrochemical Materials Laboratory, Department of Physics, Shivaji University, Kolhapur, 416004 India

*e-mail: rajpure@yahoo.com

Received December 1, 2020; revised January 10, 2021; accepted January 10, 2021

Abstract—Titanium dioxide (TiO₂) and doped TiO₂ have emerged as efficient photocatalytic materials for the degradation of harmful dyes released in water. The doping significantly increases the photocatalytic activity of TiO₂ by enhancing light absorption in visible region and by alteration of structure, surface area and morphology etc. The doping of TiO₂ has been achieved with various elements from the transition metal series, ions, nitrogen, with rare earths and other metallic nanostructures. Recently, significant new developments were noticed in the literature about doping of TiO₂ with new materials using different strategies. In this review, the basic information of TiO₂ as a photocatalyst is presented and the importance of doping to improve the photocatalytic performance of TiO₂ is highlighted. Recent reports about the doped TiO₂ from the literature are listed in tabular format and critically analyzed. The collective information presented will help to design new doping strategies and to come up with novel and more efficient TiO₂ based photocatalysts to develop a water purification technology.

DOI: 10.1134/S2635167622010104

1. Introduction
2. Titanium dioxide as a photocatalyst
3. Doped Titanium dioxide and its advantages
 - 3.1. Metals
 - 3.1.1. Doping
 - 3.1.2. Codoping
 - 3.1.3. Composites
 - 3.2. Non-metals
 - 3.2.1. Doping
 - 3.2.2. Codoping
 - 3.2.3. Composites
4. Conclusions and future prospects

1. INTRODUCTION

The increased industrialization all over the world has caused serious environmental issues, affects the life of people as large amount of the industrial effluents containing hazardous waste such as dyes are disposed directly into water bodies. These effluents violate the environmental sustainability [1, 2]. According to estimation of World Bank, the major contributors for water pollution are the dyeing and textile industries. They contribute about 17–20% of the total water pollution [3]. The pollutants may have very adverse effect on human health. For instance, certain organic pollutants present in water above the allowed concentration levels can harm the human system. In addition

to humans, marine entity as well as to various useful microorganisms get affected by most of the dyes present in water. To tackle this serious issue, most of the different techniques like physical, chemical and biological methods where scientists are working on decontamination of water bodies [4]. However, it is observed that these techniques are inefficient and have various constraints such as high cost or need of reprocessing of the materials used etc. Therefore, there is need to develop a feasible and an economic technique for removal of such unsafe pollutants from water [5, 6]. There do exist some biological water treatment but they also have their limitations. The biological methods can be substituted by heterogeneous photocatalysts for dumping of the pollutants by their photodegradation [7]. Recently, there is great interest in the use of TiO₂ based photocatalysts for the degradation of dyes in water.

In recent years, advanced oxidation processes (AOPs) are promising, efficient and ecofriendly methods flourished to oxidize pollutants from wastewaters [8]. Photocatalysis has become an essential part of the AOPs, which is an in situ chemical method (oxidation) to remove organic (and sometimes inorganic) materials present in water by oxidation through reactions with highly reactive hydroxyl radicals ($\cdot\text{OH}$) [9]. These radicals are built up with the help of catalysts (e.g. TiO₂). The major organic compounds that comprise the industrial wastewater include dyes, carbox-

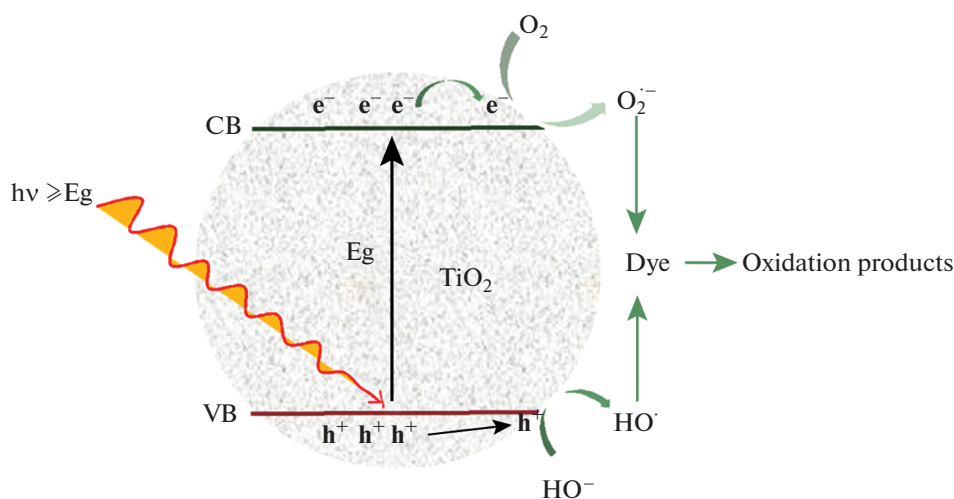


Fig. 1. The photocatalytic dye degradation process assisted by TiO₂.

ylic acids, phenols, chlorophenols, aliphatic alcohols, aromatics, and polymers. Among those, methylene blue (MB) [10], toluene [11], salicylic acid (SA) [12] and 4-chlorophenol (4-CP) [13] etc. are discharged from industries in water bodies including paper milling, textile, cosmetics etc. The presence of these compounds in water cause awful odor to the water. Therefore, a large number of semiconductors have evolved as photocatalysts to degrade these dyes and compounds mentioned above [14].

Photocatalysis is employed in various area such as solar cells [15], water splitting [16], and pollutant degradation [17]. Photocatalysis plays a significant role for degradation of organic compounds into less harmful compounds like CO₂ and H₂O etc. The generation, dissociation, recombination, and surface capture of photogenerated electrons and charge carriers (e⁻/h⁺ pairs) are the main steps tangled in photocatalytic process [18]. Photocatalytic reactions occur on the surface of semiconductors [19]. The basic operations of the photocatalytic process comprise the reduction and oxidation reactions, along with some secondary reactions, which set up the driving force of a number of main photocatalytic applications as shown in Fig. 1 [20]. For the oxidation of various organic compounds such as Methyl orange (MO), Congo red (CR), bisphenol A, tetracycline etc. a photocatalytic process utilizing a semiconductor as photocatalyst (ex. TiO₂) under UV irradiation [21].

A semiconductor electrode should meet some prerequisites such as suitable band gap and appropriate valence and conduction band (CB) positions relative to water oxidation and reduction potential where OH radicals and O₂⁻ are generated at respective electrode upon incidence of photon. For energetically conceivable water splitting reaction the CB of the semiconductor should be more negative than reduction poten-

tial of H⁺/H₂, and the valence band (VB) maximum should be more positive than the oxidation potential of O₂/H₂O. Therefore, the band gap energy of photocatalyst should be more than water splitting potential 1.23 eV with suitable band position. The band edge positions of various semiconductors relative to water redox potential are shown in Fig. 2 [22]. Among various semiconductors, the strong oxidation ability of photo-excited TiO₂ has gained more attention due to its intrinsic properties [8] such as TiO₂ is an inorganic semiconducting metal oxide, efficient for degradation of pollutants received to its enormous advantages including its high photocatalytic activity, good chemical inertness, non-toxicity, low cost and strong chemical stability in a large pH range [23]. TiO₂ exists in three polymorphs such as rutile, anatase and brookite. Anatase phase is recommended due to its high electron affinity, more effectiveness for best catalytic performance [24]. The mechanism of photocatalysis in TiO₂ reported elsewhere [25]. The photocatalytic performance and recombination rate of carriers in TiO₂ depends on its crystallinity, size, and surface area [26].

However, the use of TiO₂ for industrial application is inadequate due to its activation under ultraviolet light (UV) irradiation, its wide band gap, high recombination, and weak separation efficiency of carriers [27]. Various strategies were adopted to enrich the performance of photocatalyst towards red shift [28] i.e. to broaden absorption of the light to the visible region [29]. Doping is an effective method. The life time of carriers is increased by dopants which act as electron hunters. Doping of TiO₂ with transition and rare earth metals has received much attention for improving the photocatalytic performance [30]. For instance, the photocatalytic degradation of dyes having pure, Ce and Mn doped TiO₂ were assessed by using Langmuir–Hinshelwood (LH) kinetic model where photo-

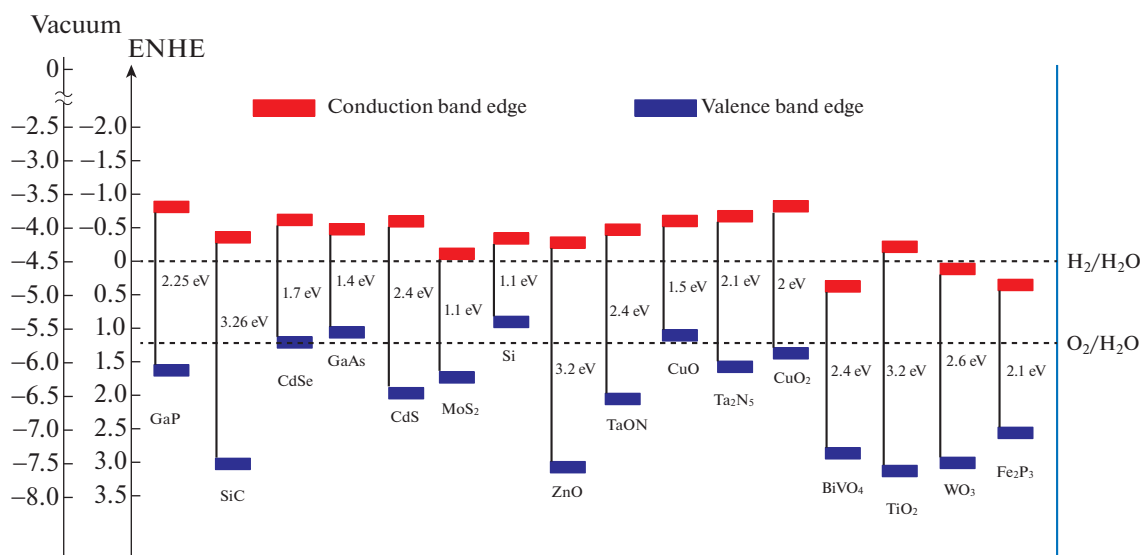


Fig. 2. Various semiconductors band edge positions in contact with aqueous electrolyte at pH 0 relative to vacuum and NHE. Reproduced with permission from [22]. Copyright ©2016 Royal Society of Chemistry.

degradation rate of dyes follows pseudo-first-order rate [30]. Li et al. [31] summarized palladium enhanced plasmonic photocatalysis. Juma et al. [32] studied Zr-doped TiO₂ thin films employing the chemical spray pyrolysis (CSP) method to scrutinize the effect of doping on their properties for application as a dielectric layer in thin film transistor.

In this review, basic information about TiO₂ based photocatalysts is presented followed by the detailed explanation of doping strategies. The latest reports from the literature about the synthesis and use of doped TiO₂ for dye degradation are collectively reported in tabular form to provide the readers with important achievements at a glance.

2. TITANIUM DIOXIDE AS A PHOTOCATALYST

Among all semiconducting materials, TiO₂ is the most popular semiconductor used as photocatalyst due to its unbeatable properties as discussed earlier as high chemical stability, non-toxicity, high reactivity, low cost and anti-corrosive property [33]. It works in UV region, with wide band gap (approximately 3.0–3.2 eV). It has very unique properties such as strong capacity of oxidation and strong affinity for water. As discussed earlier, TiO₂ appears in three polymorphs: rutile (tetragonal), anatase (tetragonal) and brookite (orthorhombic) [34]. A light of wavelength 415 nm is captivated by rutile phase. Whereas near-UV region, light of wavelength 385 nm is captivated by anatase phase. Different methods are used to synthesize TiO₂ photocatalyst such as sol-gel method, atomic layer deposition (ALD), chemical vapor deposition (CVD), spray pyrolysis, flame hydrolysis, plasma assisted

pyrolysis, mechanical alloying, metal organic chemical vapor deposition, hydrothermal methods, the wet impregnation technique etc [35–37]. Based on the growth process the structural, optical and electronic properties of TiO₂ changed. From the structural point of view, these materials are usually nanocrystalline in a network of oxide particles implying their electronic structure where the pavement of charge carriers is depend on the electronic structures of oxide materials (TiO₂) [38]. The development of various Ti-oxide-based photocatalytic materials, the underlying reaction mechanisms and kinetics were analyzed by using a number of molecular spectroscopies.

In photocatalysis, absorption of UV light by semiconductor is followed by the charge carrier-pairs (electrons (e⁻) and holes (h⁺)) separation and interfacial charge transfer (CT). Generally, without O₂ the photocatalytic degradation of organic compounds does not proceed [20]. In actual process, Water adsorbed on the surface of TiO₂ reacts with holes to produce hydroxyl radicals ([•]OH) and electron reacts with O₂ to produce superoxide anions (O₂^{•-} and [•]OH) which helps to deteriorate organic pollutants exist in the water [18]. The transfer of electrons from VB to CB via band to band transitions is allowed by leaving behind hole in VB. Generally, electrons are trapped at the surface and in the bulk of TiO₂. Once the electrons gets trapped, Ti⁴⁺ cations are reduced to Ti³⁺ states and the holes oxidize O₂⁻ anions to O⁻ states [39]. So often the charge carrier kinetics determines the photocatalytic efficiency. TiO₂ is a mixture of 80% anatase and 20% rutile [34]. Anatase has a shallow donor level, high electron mobility, and more defects in the lattice, producing more oxygen vacancies and capturing the

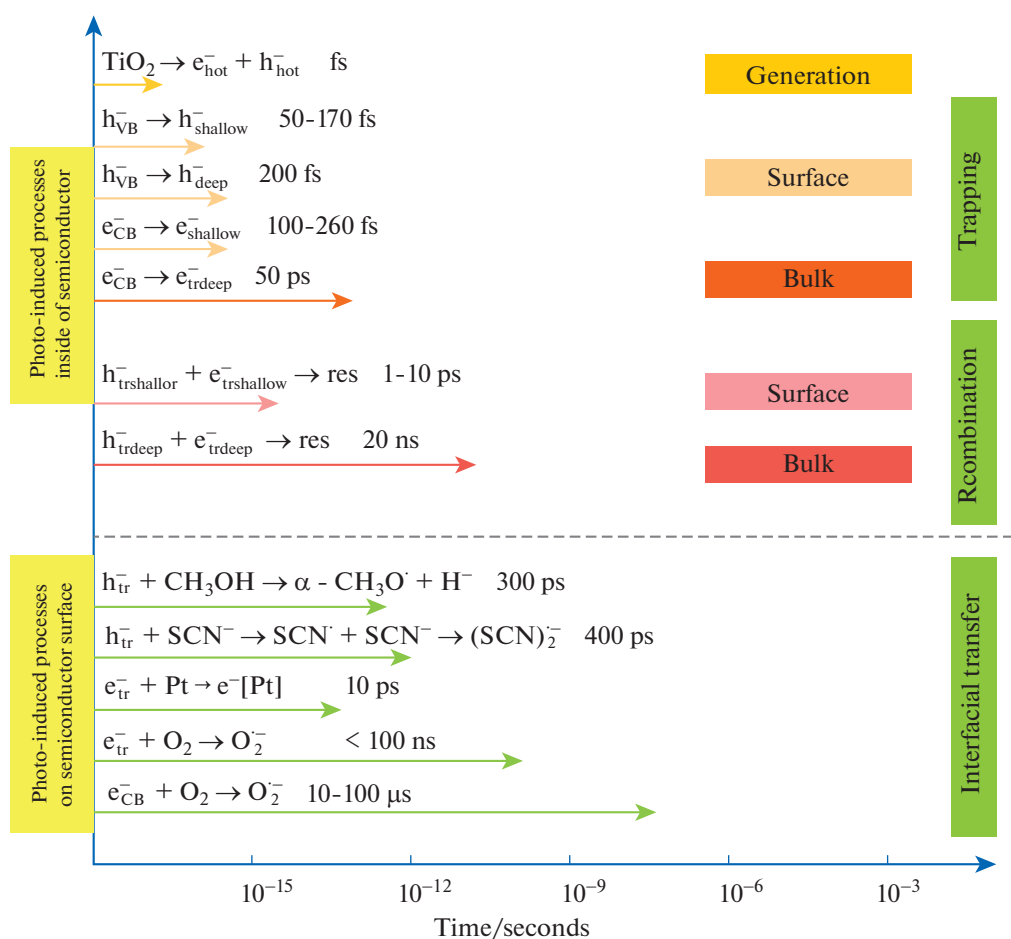


Fig. 3. The time scales and oxidative reactions in TiO_2 photocatalysis. Reproduced with permission from [45]. Copyright 2014 American Chemical Society.

electrons [40]. Therefore, there is a higher proportion of anatase, the form of TiO_2 which absorbs UV light, used for applications in photocatalysis, water splitting and dye-sensitized solar cell. Diebold et al. [41] reported most stable anatase TiO_2 particles of band gap of approximately 3.2 eV. The detailed electronic and optical properties of TiO_2 in the anatase structure reported elsewhere [42] where molecular orbital structure helps to find out the band structure, density of states (DOS) and charge densities. The VB of TiO_2 is constructed by energetic O p at the top level of the valence band. Meanwhile its CB is from Ti 3d and 4s. Such unique electronic structure in anatase TiO_2 has led to the high mobility of n-type charge carriers [43]. It displays a more surface adsorption capacity to hydroxyl groups and a lower charge carrier recombination rate which is much better for photocatalytic activities [44].

The photoinduced reaction occur inside and on TiO_2 surface in the time scale region from femtoseconds to microseconds are illustrated in Fig. 3 [45]. Moreover, the reaction occurs on the surface of the

material and surface reactivity affects the catalytic performance of the material.

TiO_2 at nanoscale having the high surface area, and more active sites (Fig. 4). Its reactivity is associated with its particle shape, which vary according to the preparation condition. The anatase TiO_2 has the {101} surface facet, for which only 50% of the Ti atoms are five-coordinated (Ti5c), both the {001} and {100} surfaces facets consist of 100% Ti5c atoms. These atoms act as active sites in the photocatalytic experiments, so by this reason, the facets {001} and {100} should be more active than {101} facets [40]. TiO_2 can be prepared in mobilized and immobilized form via different techniques on which different properties are reliable which are beneficial for photodegradation. The pH value also influences different properties in photodegradation process. Under high acidic OR basic conditions, reactions are not favored. Where at optimal pH, hydroxyl groups on the surface of TiO_2 producing OH radicals by speeding the oxidation of pollutant using OH^- groups and improve the photocatalytic efficiency [46]. In spite of all TiO_2 properties and the good photocat-

alytic performance, its use is hindered due to its low adsorption, results in low catalytic efficiency. The bottleneck in photocatalysis is to enhance efficiency by alleviating the present limitations. The following discussion is focused on the enhancement of photocatalytic performance of TiO₂ by new doping strategies.

3. DOPED TITANIUM DIOXIDE AND ITS ADVANTAGES

Although TiO₂ has a wide range of applications in photocatalysis, its use is hindered due to its wide band gap, low light utilization efficiency and high carrier-recombination rate. Various possible ways improve the photocatalytic activity and shift the action of TiO₂ to visible range. One of the possible way to solve this issue is by changing the interfacial charge through the doping process. Doping is an unusual way to alter the surface morphologies (nanowires/nanotubes/nanoparticles), chemical modifications (incorporation of additional components in the TiO₂ structure) and particle size of photocatalyst [47]. The main intend of doping is to change its large band gap and electronic structure; reducing recombination of photogenerated charge carriers, and enhancing surface and interface characteristics. The crystal lattice face can be inflected by doping [29] where photoactivity strongly depends on the crystal faces. Hence, its photocatalytic applications can be enhanced by shifting the absorption edge of TiO₂ towards the visible region (400–800 nm). Doping hampers the charge recombination and ameliorates photocatalytic activity [48]. Low et al. [49] reported the surface modification of TiO₂ for photocatalytic CO₂ reduction via impurity doping, metal deposition, alkali modification, heterojunction construction and carbon-based material loading. Black phosphorus doped TiO₂ nanotubes leads to the production of promising materials. Compared to pristine anatase 3.2 eV TiO₂ nanotubes, the creation of heterojunctions in the hybrid material results in 1.5–2.1 eV photoelectrocatalysts [50]. Similarly, co-doping and tri-doping different metals as well as a mixture of metals with non-metals have been more effective than mono-doping, in certain cases, for increasing visible-light absorption [51–53]. Ullattil et al. [54] developed Mn(II) assisted sol solvothermal technique for the synthesis of positively surface charged defective brown TiO_{2-x} flower aggregates with porous nature. Moreover, the photocatalytic efficiency of these materials have been carried out using methyl orange-methylene blue (MO-MB) dye mixture model system under solar irradiations shown in Fig. 5, resulted in the selective photocatalytic reversibility such that MB and MO photodegradation have been selectively performed by yellow TiO₂ and brown TiO_{2-x} respectively. Different strategies have been adopted to alter TiO₂ for improvement in photocatalytic efficiency by utilization of visible light. Stabiliza-

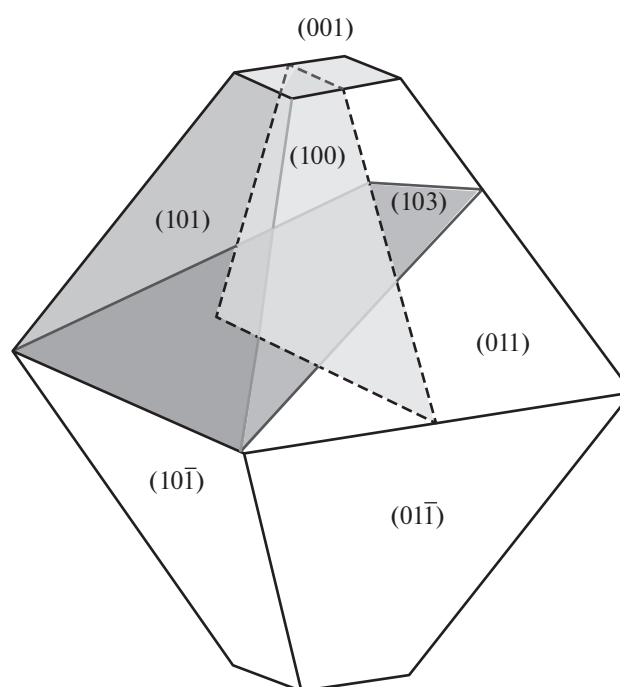


Fig. 4. Various Crystallographic places of anatase TiO₂ crystal in equilibrium shape. Reproduced with permission from [41] Copyright 2003 Elsevier.

tion of the anatase form is carried out in different ways; one of them is cationic or anionic doping of the material, dye sensitization, coupling semiconductors and creating heterojunctions based on it are some of the most efficient ways to overcome this drawback.

3.1. Metals

3.1.1. Doping. The doping of TiO₂ especially with metals enrich its electronic and optical properties. Amongst a potential effect in metal doping is the shifting of the energy band gap of the anatase TiO₂ to the visible region, creates carrier trap density and oxygen vacancy or increasing the free-carrier density. This effect increases the photosensitivity of the anatase TiO₂. It improves the performance of TiO₂ in photocatalysis, sensing, dye sensitized solar cell etc. [43]. The most commonly used metal dopants are alkaline earth metals, transition metals (Fe, Mn, V, Cu, and Cr, both delocalized and localized impurity states), post-transition metals, and rare earth (RE) metals. Among transition metals, first-row transition metals as well as d8 and d9 transition metals are most commonly employed, where the 3d orbitals of the dopant metal introduce electronic states in between the original band gap.

Alkali- Alkaline earth metals. Among all the doping strategies, several papers have reported based on alkali-earth-metal doping with the mechanism for the enhanced photoactivity. The systematic understand-

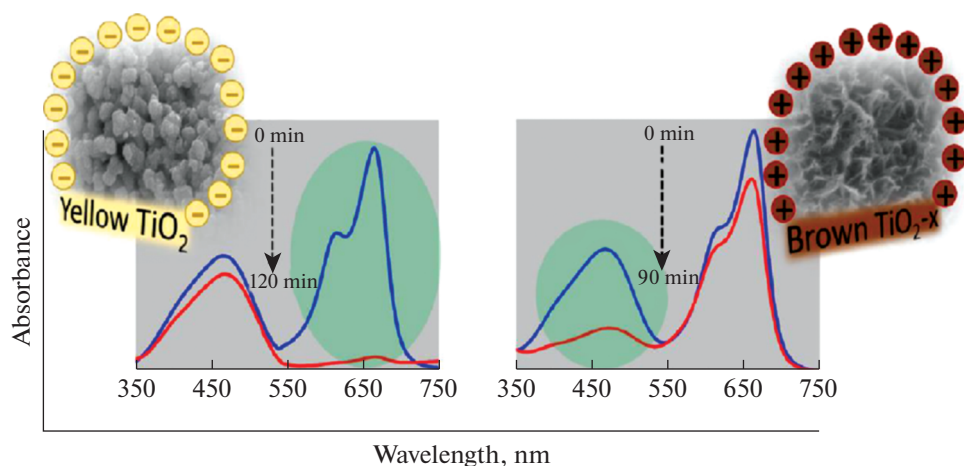


Fig. 5. UV-Visible absorption spectra of photodegradation of MO and MB using TiO_2 (yellow) and TiO_{2-x} (brown). Reproduced with permission from [54]. Copyright 2018 American Chemical Society.

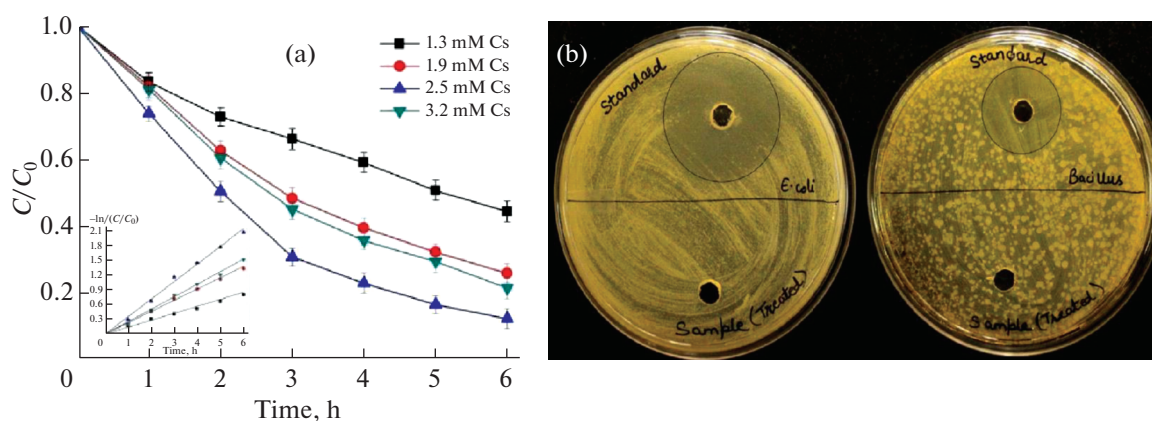


Fig. 6. Influence of Cesium concentration (0.02 A Current , $150 \text{ mg L}^{-1} \text{ Na}_2\text{SO}_4$) and pH on the degradation of 4-CG (a). Results of toxicity treated 4-CG solution against *E. coli* and *B. subtilis* (b). Reprinted with permission from [56]. Copyright 2019 Elsevier.

ing and mechanism of the doping effect of alkali earth metals on TiO_2 to improve the photoactivity has studied. AM- TiO_{2-x} (Mg, Ca, Sr, and Ba) with different doping contents were prepared and tested in photodegradation. Lv et al. [55] reported alkaline-earth-metal (Mg, Ca, Sr, and Ba) doped TiO_2 to furnish the photodegradation and H_2 evolution with honeycomb-like inverse opal structure. Subsequently both the CB and VB of TiO_2 were switched to more negative values, which subscribed to the formation of O_2^- , emanating in photodegradation (RhB) being significantly promoted.

Rajput et al. [56] synthesized a novel Caesium (Cs) loaded TiO_2 nanotube ($\text{Cs}/\text{TiO}_2\text{NTs}$) electrode by anodization method for the removal of 4-chloroguaiacol (CG). A comparative evaluation between photoelectrocatalytic (PEC), photocatalytic (PC) and electrocatalytic (EC) process where $\text{Cs}/\text{TiO}_2\text{NTs}$

(2.5 Mm) showed highest PEC activity than bare TiO_2 electrode in terms of (92%) degradation of 4-CG in 6 h under sunlight and mineralization ($\text{TOC} = 70.2\%$) as shown in Fig. 6a. The boost in degradation rate constant was due to Schottky barrier at the interface of metal and semiconductor facilitating the reduction in rate of recombination of charged species. Also the successful PEC treatment of 4-CG also confirmed by toxicity test which did not showed any toxic effects against the selected bacterial species (*E. coli*, *Bacillus*) as shown in Fig. 6b.

Transition metals. A transition metal is an element whose atom has an incomplete d sub shell or it can give rise to the cations with an incomplete d sub shell. There are also several reports about the transition metal doped TiO_2 materials for photocatalytic applications. Li et al. developed a novel method, hydrodynamic cavitations (HC) combined with Fe^{3+} -doped

TiO₂, for the degradation of Rhodamine B (RhB). The reaction mechanism of Fe³⁺-doped TiO₂ is as discussed in [57]. Moreover, doping of Fe into TiO₂ lattice forming Fe³⁺-doped TiO₂ to further improve the catalytic performance of TiO₂ by catalytic degradation of RhB. Fang et al. [58] revealed the synergistic study between Ti³⁺ self-doping and dual-facets exposure results in the more photocatalytic performance for degradation of RhB and formic acid under solar irradiation. The dual facets which act as holes and electrons collectors separate the charges of the reduced TiO₂ catalyst. Qiu et al. [59] developed new idea for the design of surface Oxygen vacancies enriched semi-conductive catalysts Pt-Ovs/Ti³⁺/TiO₂ (PVTT) for photocatalytic degradation of Acid Orange II (AO₇) which shows photocurrent density and rate constant are about 3.9 times and 4.44 times higher than that of Pt-TiO₂. Natarajan et al. [60] and Li et al. [61] prepared Bi-doped TiO₂ to increase the photocatalytic activity for the degradation of different organic pollutants. The higher mineralization of sulforhodamine-B (61.6% of TOC removal) and degradation rate of RhB (more than 90 at 0.25% of Bi-TiO₂) had been recorded under visible light. The incorporation of Bi induces the Bi⁴⁺/Bi³⁺ species, which ensure the separation of the electron-hole pairs. Santamaria et al. [35] reported sol gel synthesized Fe (5 wt %) doped TiO₂ where the Fe favors the action of TiO₂ in the degradation of SA under UV light. Hinojosa-Reyes et al. [62] reported titania doped (Ni, Cu, and Fe) nanomaterials were synthesized by sol gel method to degrade 4-chlorophenol (CP) and naproxen (NPX) sodium as pollutants under UV illumination. The photocatalysts: T-Cu 1.0 and T-Fe 1.0 were degraded 4-CP (90%) and NPX (97%) pollutants in 6 hr, shows remarkable catalytic performance due to a higher concentration of Ti³⁺ species.

Localized Surface Plasmon Resonance (LSPR)-induced absorption in the visible region was successfully achieved by Mo-TiO₂ and W-TiO₂. The free electron concentration in Mo-doped TiO₂ nanocrystals was comparable to noble metals, and the peak shape closely resembled **that for** Au NPs. On the contrary, the LSPR peak of W-doped TiO₂ was much wider, covering a larger portion of the visible to near-IR regions. It is observed that on varying the size (13–5 nm) of the W-doped nanocrystals, gave rise to a blue-shift in the peak maximum from 1700 to 980 nm [63]. Takle et al. [64] reported sol gel based V-TiO₂ photoelectrode for degradation of spent wash and Jakofix red dye under natural sunlight using aqueous titanium peroxide with titanium isopropoxide as the Ti precursor and V₂O₅ as the V precursor. Optical study showed red shift in the absorption edge of TiO₂ upon V doping narrow the band gap. Therefore, the absorp-

tion band (Fig. 8) observed in the visible region due to V⁴⁺ and V⁵⁺ states in TiO₂.

Figure 7I shows the degradation of color with variously doped TiO₂ material. From Fig. 7II, it is quite evident that the degradation of spent wash was 54 and 65% under the Xe lamp and natural sunlight respectively. The color degradation rate was faster under sunlight than under a xenon lamp as luminous efficiency under sunlight is higher than that of Xe lamp. The photocatalytic activity of a 1% V-TiO₂ catalyst in the degradation of Jakofix red dye (100 ppm solution) shows 90% of Jakofix red dye degraded under solar radiation after 3.5 h which is more than that pure TiO₂ and Dessuga P-25 shown in Fig. 7III. The increase in photocatalytic activity showed the combined effect of the doping of V into TiO₂ and the hierarchical nanostructures formation in V-doped samples.

Rare earth metals. Electronic and crystal structure of TiO₂ can be changed by RE elements as dopants due to their 4f electronic configuration and spectroscopic properties. Electrons in CB of TiO₂ were trapped by lanthanide ion where it acts as electron scavenger. Moreover, researcher studied doping of TiO₂ with RE ions (S³⁺, Ce³⁺, Er³⁺, Pr³⁺, Gd³⁺, Nd³⁺, and Sm³⁺) which improved photocatalytic activity in the degradation of nitrite. The doping with lanthanide ions (La³⁺, Er³⁺, Pr³⁺, Nd³⁺, and Sm³⁺), improves the photoelectrochemical properties as well as increased the photocurrent response and the photon current conversion efficiency in the range of 300–400 nm [65]. Stengl et al. [51] reported the synthesis of rare earth (La, Ce, Pr, Nd, Sm, Eu, Dy, Gd) doped TiO₂ by sol gel method where Nd³⁺-doped TiO₂ (approx. 10 wt %) shows the best photocatalytic activity among all rare earth doped samples due to the transitions of 4f electrons of rare earth and red shifts of the optical adsorption edge of titania and dye sensitization enhanced visible-light photocatalytic activity of TiO₂. Pawar et al. [66] reported case study on degradation of MB dye using Ce-TiO₂ photocatalysts. Ce-TiO₂ is more catalytic to oxidize it from Ce³⁺ to Ce⁴⁺ states. Redox couple of Cerium (Ce³⁺/Ce⁴⁺) shifts between CeO₂ and Ce₂O₃ under redox conditions which makes it active under UV-Vis range. Therefore, its optical as well as catalytic properties is changed by different electronic structures between Ce³⁺ and Ce⁴⁺. Reli et al. [67] reported synthesis of novel cerium-doped TiO₂ with sol-gel method within surfactant Triton X-114 in cyclohexane and showed 1.2 wt % Ce gives the maximum photocatalytic activity for the decomposition of ammonia under UV light radiation. Phattepur et al. [68] developed bare and Gd doped (0.5, 2, 4 and 6 wt %) TiO₂ thin films by sol-gel and spin coating techniques for the degradation of RhB (99%) in 50 min under UV illumination. Choi et al. [69] synthesized three-dimensional (3D) Gd-doped TiO₂ nanofibers using a

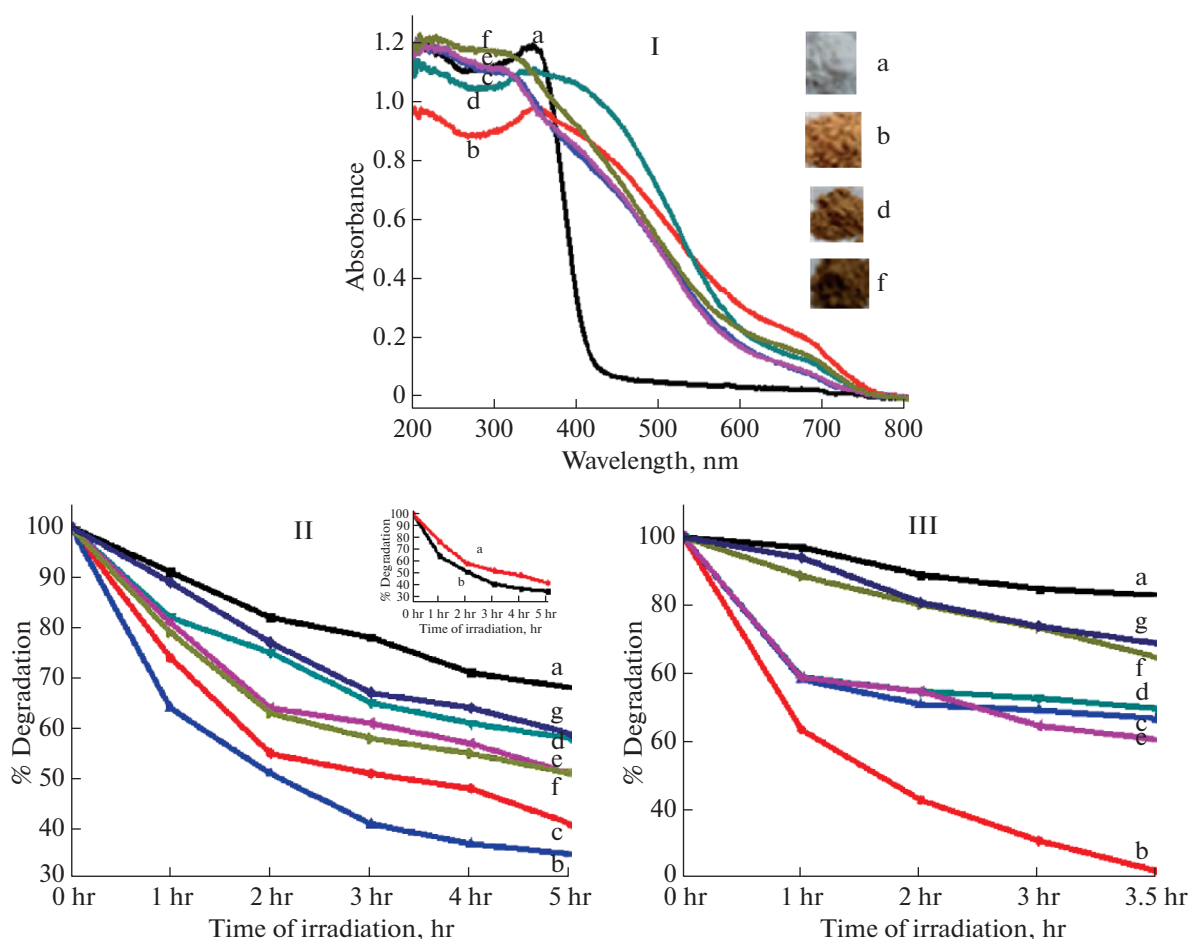



Fig. 7. UV-Visible DRS spectra (I) of samples a – TiO₂, b–f – 1–5% V–TiO₂. Degradation of color in spent wash (II) and dye (%) (III) after irradiation with sunlight: a – Undoped TiO₂, b – 1–5% V–TiO₂, c – P-25 TiO₂. Inset in (II) shows 1% V–TiO₂ spent wash degradation (a) under xenon (b) under sunlight. Reprinted with permission from [64]. Copyright 2018 Royal Society of Chemistry.

simple electrospinning technique. SEM micrographs of Gd–TiO₂ nanoparticles and Gd–TiO₂ nanofibres along with its respective TEM images are shown in Figs. 8a, 8b. The Gd-doped TiO₂ nanofibres showed a higher photocatalytic activity as well as nearly five-fold raise in the photocatalytic degradation rate due to higher electron transport than  TiO₂ nanoparticles due to the fast electron transport and •OH production as shown in Fig. 8c.

3.1.2. Codoping. The co-doping is an effective strategy that can be used for tuning the dopant populations and electronic properties of a material. The physicochemical properties of sol-gel and hydrothermally prepared new bimetallic Cu–Ni/TiO₂ photoanode by varying calcinations duration (60, 90, 120 min) showed enhanced crystallinity, diminished CT resistance as well as better photocurrent densities for solar hydrogen production (SHP) [70]. The synergistic effect of Zr, Ag codoped TiO₂ promoted decolorization of MB dye under fluorescent light, with the high-

est degradation efficiency (98%) as well as the improved antibacterial (*E. coli*) efficiency [71]. The details of decoloration efficiencies from this report are presented in Table 1.

There are also various examples in the literature about co-doped TiO₂ synthesis and its use as efficient photocatalyst. Lv et al. [72] reported the photodegradation activity of MB by V, Co codoped TiO₂ via sol-gel method, indicates MB degradation in one hour with efficiency to be 92.12% which is more than Desugga P-25. The increase in efficiency is due to lattice distortion by co-doping of V and Co ions. XPS analysis showed shift of Ti 2p_{3/2} and Ti 2p_{1/2} peak towards higher binding energy by V, Co doping in TiO₂, which is due to the transfer of electrons from Ti⁴⁺ to V⁴⁺ and Co²⁺. Iihoshi et al. [73] synthesized composite photocatalysts with copper ion loaded tungsten trioxide (Cu/WO₃) and copper ion loaded nitrogen-doped titanium dioxide (Cu/N–TiO₂) to study the photocatalytic activity by decomposing acet-

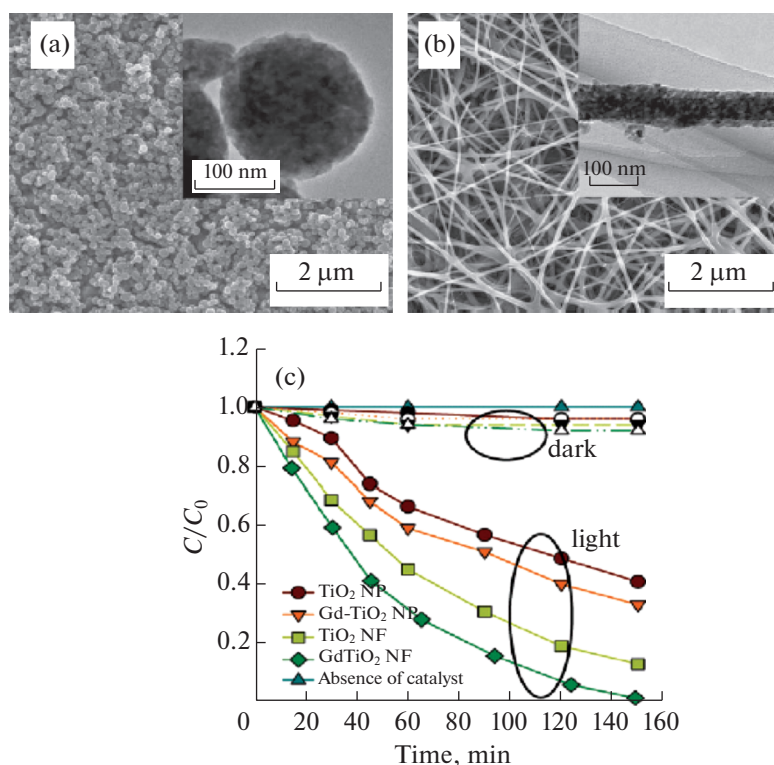


Fig. 8. SEM micrographs of Gd-TiO₂ nanoparticles (a), Gd-TiO₂ nanofibres and insets represents TEM images of respective electrode (b), Photocatalytic dye degradation (MO) response of pristine (c), G-TiO₂ nanoparticles and nanofibres under visible light illumination. Reproduced with permission from [69] Copyright 2014 The Royal Society of Chemistry.

aldehyde gas under visible light by time resolved visible to mid infrared (IR) spectroscopy. It showed enhancement in catalytic activity due to longer hole lifetime. A novel Ni²⁺ and Ti³⁺ codoped porous anatase TiO₂ was developed by Zhang et al. [74] via a facile sol–gel technique combined with an in situ solid-state chemical reduction approach accompanied by mild calcinations (350°C) in Ar atmosphere. The doping of Ti³⁺ and Ni²⁺ species in TiO₂ results in narrowing the band gap of anatase TiO₂. Codoped (Ti, Ni) porous black ana-

tase TiO₂ resulted in higher photocatalytic performance for MO and RhB respectively.

3.1.3. Composites. Transition metals. The introduction of transition metal ions in TiO₂ leads to an intermediate steps between the band gap, changes the carrier concentration by trapping electron hole pairs. This suppresses the electron hole pairs recombination rate and boost the degradation performance. Therefore, the photocatalytic performance of TiO₂ is effectively improved through transition metal composites [29]. El-Yazeed et al. [75] reported the mesoporous

Table 1. De-coloration efficiencies and Kinetic rate constants of Zr, Ag co-doped TiO₂ under UV and Visible light

Samples	UV		Fluorescent light	
	Kinetic constant, h ⁻¹	De-colorization efficiency, %	Kinetic constant, h ⁻¹	De-colorization efficiency, %
TiO ₂	0.4045	98.11	0.0080	11.38
A ₅ T	0.0966	65.48	0.0197	29.52
Z ₅ T	0.5753	98.98	0.0287	42.63
Z ₁₀ T	0.7207	99.14	0.0481	62.52
Z ₅ A ₅ T	0.2437	98.24	0.1250	95.16
Z ₁₀ A ₅ T	0.5443	98.07	0.2274	98.07
Z ₁₅ A ₅ T	0.5264	98.11	0.2212	98.61

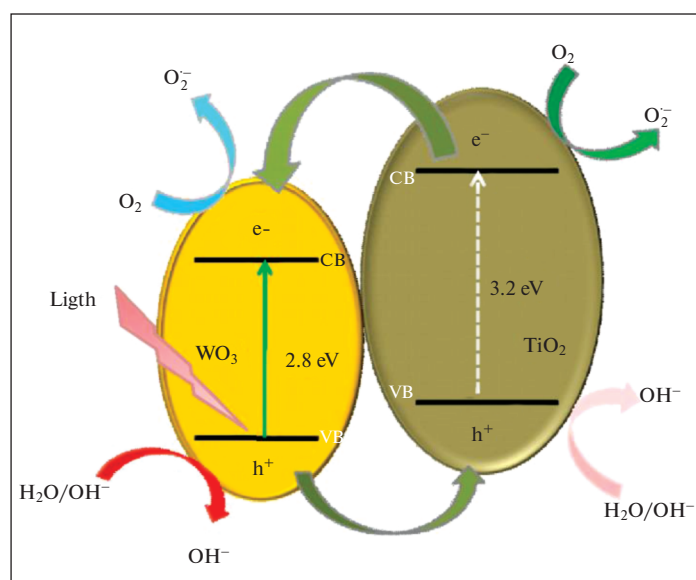


Fig. 9. Schematic of charge transfer mechanism of photoexcited WO_3/TiO_2 composites. Reproduced with permission from [75]. Copyright 2019 Elsevier.

WO_3/TiO_2 photocatalysts with different loadings of WO_3 (5, 10 and 15) wt % were used to remove MB from aqueous solution. The presence of hydroxyl groups yield OH (%) confirmed by FTIR analysis onto the surface of the sample enhances the photodegradation of MB to 99% in 3 h and in addition TiO_2 decrease the band gap energy from 3.11 to 2.92 eV (Fig. 9). It is confirmed from the result that the photocatalytic degradation of MB follows the kinetics of the pseudo-first-order model.

Liu et al. [76] fabricated dense and uniform $\text{Cu}_2\text{O}/\text{TiO}_2$ composite films by different methods (Sol-gel, Spray pyrolysis and Hydrothermal), shows the highest efficiency for photocatalytic degradation of MB dye due to reduction in band gap and larger surface area. Hossain et al. [77] synthesized multiwalled carbon nanotubes (MWCNT) coupled with silver- or iron-doped TiO_2 via a facile two-step sol-gel route at low temperature. Incorporation of metals (Fe, Ag) and CNT in the TiO_2 matrix inhibits recombination of e^-/h^+ pairs, resulting in improved efficiency which reduces the band gap and high adsorption capacity of the CNT. These results show that the SCT nanocomposite thin film may show enhanced effects for MB degradation catalyzed by TiO_2 as well as adsorption of MB by CNTs. In addition, SCT also clearly acted as a strong disinfectant for use in environmental protection applications. Li et al. [78] developed novel ternary $\text{MoS}_2/\text{MoO}_3/\text{TiO}_2$ visible catalysts for evaluating the visible photocatalytic performance of the composites for degradation of RhB under visible-light. Over 90% RhB was photodegraded under visible light irradiation due to the novel band alignment of the composite

which restrained the recombination of electron-hole pairs (O_2 and h^+).

Rare earth metal. Compared to transition metals, RE metals are considered to be as an ideal to modify crystal structure and optical and electronic properties of TiO_2 . To achieve above mentioned goal, other way to improve photocatalytic performance is RE composite. TiO_2 nanomaterials include most of the metals from Lanthanide series and most research on TiO_2 -lanthanide composites is limited to a few applications. TiO_2 composites with La_2O_3 have been investigated for catalysis in reactions such as NO_x reduction. However, there are few reports on TiO_2 composites with Er_2O_3 , Nd_2O_3 , and Eu_2O_3 . Therefore, CeO_2 has attracted more attention to improve both the UV and the visible photocatalytic degradation of organic molecules [79]. Zhan et al. [80] reported synthesis of RE (Nd) ions doped $\text{TiO}_2/\text{SiO}_2$, combining with meso-porosity and sulfation, can enhance photocatalytic activity in the degradation of MO. Photo-degradation results revealed, RE-doped samples could greatly improve the photocatalytic activity, and the experimental degradation rates were higher than that catalyzed by undoped samples and Degussa P-25, obeyed the order of $\text{Nd}^{3+} > \text{La}^{3+} > \text{Y}^{3+}$. Nd-doped sample expressed the highest photoactivity. The increase in activity is probably due to the higher adsorption, red shifts, and prevention of electron-hole pairs recombination. There are some disadvantages of metal ion doped photocatalysts. For instance, the metal-doped nanomaterials suffered from unstable optical properties and thermal instability, in addition to the need to use expensive ion implantation equipment to produce these sophisti-

cated materials. Furthermore, the localized *d*-electron state formed in the band gap of TiO₂ may become the recombination center of photogenerated electron–hole pairs, thereby leading to a decline in the photocatalytic activity [18].

3.2. Non-Metals

The non-metal dopant can substitute either at the oxygen or parent metal atomic sites, or also exist as an interstitial dopant. The *2p* orbital contributions from these non-metal dopants gives rise to the creation of mixed or localized states near the edges of the VB or CB that can lead to the narrowing of the band gap and visible light activity. The incorporation of anion species in the titania structure leads to the extension of TiO₂ optical absorption towards visible region through the formation of intragap energy states. The most commonly used non-metal dopants are nitrogen, carbon, phosphorus, fluorine, chlorine, iodine, sulfur and other tellurides such as selenium and tellurium.

3.2.1. Doping. There are several examples in the literature about doping TiO₂ with non-metals. Vasu et al. [81] employed ALD technique to prepare *p*-type epitaxial bare and N-doped anatase TiO₂ (001) thin films at 300°C on Aluminum oxide (Al₂O₃) substrate. The band gap of N-TiO₂ film vary from 3.23 to 3.07 eV and the mobility and hole concentration increases. The epitaxial relation between TiO₂ and Al₂O₃ was confirmed by transmission electron microscopy (TEM). The epitaxial films exhibited a room-temperature ferromagnetism and photo-response. Atomic force microscopy (AFM) executed the smooth and granular morphology of TiO₂ and N-TiO₂ films. Xiong et al. [82] demonstrated the higher photocatalytic activity of S-TiO₂ under solar illumination as compared to that of bare TiO₂ during the photodegradation of MB dyes as the S induces the formation of well-ordered mesostructures in the films which results in a more porosity, bigger pores, hydrophilic surface, and a narrowing the band gap. Wang et al. [83] reported the tailored photocatalytic activity of S-TiO₂ under visible light irradiation prepared by a simple hydrothermal green approach for the photodegradation of RhB compared to that of bare TiO₂. It has a larger surface area as well as decreased the band gap of TiO₂ as the *3p* level of S is greater than O_{2p} orbital of TiO₂. Hosseinzadeh et al. [84] synthesized transparent Sulphur (S)-doped TiO₂ thin films by Ultrasonic-assisted spray pyrolysis technique. The morphology of the prepared sample exhibits high uniformity and monodispersity nature of film with semi-cubic nanostructures. S-doped TiO₂ thin film showed higher photocatalytic activity than pure TiO₂ under visible-light for MB dye degradation as S dopant creates few oxygen vacancies and structural defects in TiO₂ which acts as charge trapping center and

inhibits electron–hole recombination rate and narrow the band gap of TiO₂.

Rasoulnezhad et al. [85] reported the nanostructured transparent TiO₂ and N-doped TiO₂ thin films, were deposited on glass and quartz substrates by sonochemical–CVD method for photocatalytic paraxon pesticide degradation in visible light. N-doped TiO₂ has nanocubic morphology (glass) which leads to formation of stable oxidation state (Ti³⁺) where it acts as hole trapping centers because of the substitution of O atoms with N ones. The estimated rate constants calculated to be 0.0228 min⁻¹ for N-TiO₂ thin film. Samsudin et al. [86] prepared bare and N-doped TiO₂ via a sol–gel technique where incorporation of N in TiO₂ enhances the hydrophilicity of TiO₂ surface which increases the photocatalytic degradation activity of polluted water. Ti–O–N or Ti–N–O linkages induces local states above the valence band which was responsible for the visible light response and effectively narrowing of the band gap. Low content (%) of nitrogen in TiO₂ hindered the number of electron–hole trapping sites, which drives higher concentration of active radicals for atrazine degradation and mineralization. Cho et al. [87] developed highly efficient and recyclable photocatalyst made of 3D nanostructured N-doped TiO₂ monolith as seen in Figs. 10a, 10b, represents the modification in the band structure by insertion of N in TiO₂ with 3D nanostructure. The improvement in photocatalytic activity is 2.5 times more than bare TiO₂ (Fig. 10d) due to N-doping and augmentation in the performance accelerated by the 3D nanostructure.

3.2.2. Codoping. The synergistic effect of co-doping may be associated with a decrease in the recombination of electron–hole pairs in materials. The synergistic effect of N–F codoping of TiO₂ prepared by dip coating and hydrothermal method on stainless steel showed a significant effect on the PEC degradation of cyanide ions (CN⁻) from aqueous solutions [88]. These dopants (N, F) allow the activation of TiO₂ under visible light by reforming the electronic band level of TiO₂ and generate the localized states within its band gap. Therefore, the modification of TiO₂ using (NH₄F) and (TEA) precursors leads to more crystallinity of anatase phase and shows absorption edge towards red shift region. Bayan et al. [89] reported sol gel synthesized Zn–F co-doped TiO₂ nanomaterials to study the photocatalytic degradation performance of MB under UV light (99%) and visible light (96%). Furthermore, this catalyst exhibited excellent stability that's why the development of such photocatalysts may be considered a breakthrough in large-scale utilization of heterogeneous photocatalysis via visible light to address water contamination and environmental pollution.

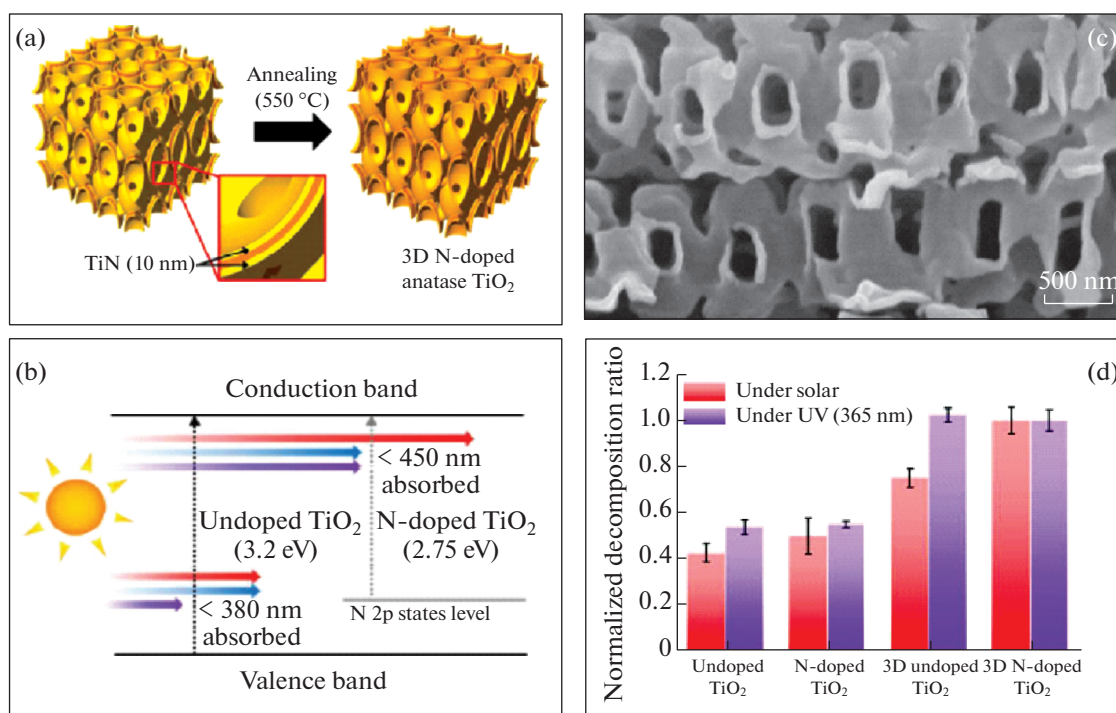


Fig. 10. Illustration of fabrication process of N-TiO₂ (a). Comparison of band energy level diagram between undoped and N-doped TiO₂ films (b). Cross-sectional view of a 3D N-doped TiO₂ film (c). Normalized decomposition ratio of MB solutions with unstructured and undoped, unstructured and N-doped (d), 3D undoped, and 3D N-doped TiO₂ films under UV and solar irradiation for 3 h. Reprinted with permission from [87]. Copyright 2018 Royal Society of Chemistry.

Kmentova et al. [90] described the synthesis of hybrid nanostructure sulfur-, nitrogen-, and oxygen-doped carbon (SNOC) nanosheets-based TiO₂ Nanorods by combined hydrothermal and spin coating technique which shows much higher photocurrent density (795 $\mu\text{A cm}^{-2}$), and enhanced the separation of photogenerated charges due to the band-bending developed at the interface between TiO₂ and SNOC. Raman spectroscopy showed crystalline structure of composite depicted with inset shows cross sectional image of TiO₂ nanorods of 1 μm length in Fig. 11a. Figure 11b shows the successful loading of SNOC1 over the titania nanorods which was studied by high resolution transition electron microscopy (HRTEM). The composites exhibits highest photoelectrochemical and photocatalytic activity towards decomposition of RhB as shown in Figs. 11c, 11d.

3.2.3. Composite. Graphene has many extraordinary properties such as high electron mobility and surface area. Over the past decades, it has studied heavily with respect to composites with TiO₂. Electron injection in graphene sheets helps to enhance the charge separation, with higher wave function ($\sim 4.9\text{--}5.2$ eV) with respect to TiO₂. By reduction of graphene oxide (GO) sheet chemical utilization of graphene has been established, which is synthesized by the Hummers

method [79]. Wang et al. [91] fabricated GO/TiO₂ (TGO-x %) composites using hydrothermal method, where GO prepared from natural graphite powder by a modified Hummers method fend off the TiO₂ nanoparticles from agglomeration. The large specific surface area and effective charge carrier separation ability of composites raised the adsorption capacity for organic pollutants. With increase of GO content, the adsorbability of TGO composite ameliorated. However, GO shows the highest adsorbability at MB. This is attributed to increase oxygen-containing functional groups and porous structure of TGO-20% composites. TGO-20% composites exhibit the synergy effect of adsorption and photocatalysis, leads to highly efficient MB degradation. The superior photodegradation activity of TiO₂/GO composites is mainly attributing to the strong absorption of visible light and the photoluminescence (PL) shows the effective charge separation. The total removal rate of MB is 97.5% after 35 min adsorption and 140 min degradation, which is 3.5 times higher than that of TiO₂. Recently, there are different reports as discussed above on metal and non-metal doped TiO₂. This comparable study of dopants helps to determine the best photocatalyst to degrade the organic pollutants.

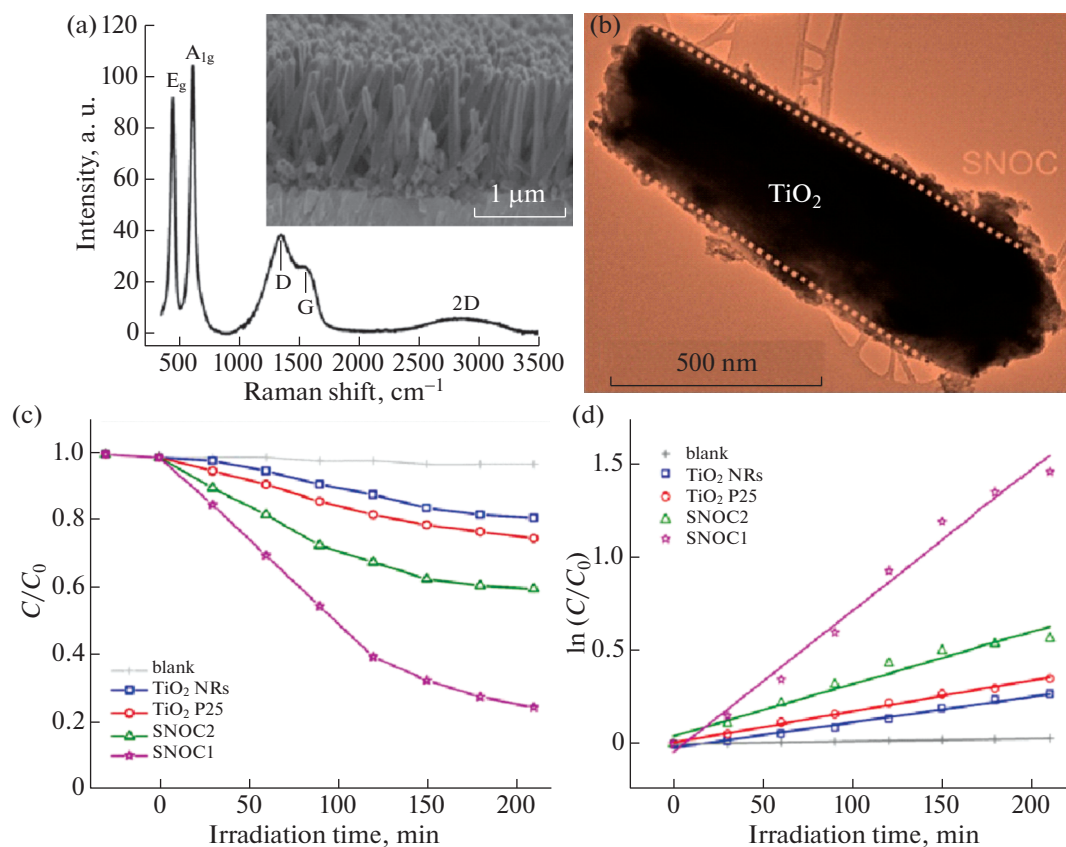


Fig. 11. Raman spectrum of TiO₂ NRs with SNOC1. Inset shows cross sectional view of TiO₂ on FTO (a). HRTEM of TiO₂ and TiO₂/SNOC (b). Photocatalytic degradation performance of TiO₂, TiO₂ P-25, SNOC1 and SNOC2 samples (c, d). Reprinted with permission from [90] Copyright 2019 Elsevier.

Recently, many works reported the use of doped TiO₂ nanostructure for the degradation of various dyes. The collective information with main observations and results from the latest reports (years 2019 and 2020 mostly) are reported in Table 2.

4. CONCLUSIONS AND FUTURE PROSPECTS

In this review, we have summarized the significance of doped TiO₂ for photocatalytic degradation of pollutants (dyes). Several different strategies have been adopted to achieve the doping of TiO₂ to transform it in to more efficient photocatalyst. One of the main disadvantages of TiO₂ photocatalyst is the need of the UV radiation for its activation. This requirement is an obstacle in terms of commercialization of this technology since it is not energy efficient. Modifications of TiO₂ can resolve this issue to some extent by narrowing the band gap and by shifting the activation wavelength in visible region. Doping seems to be an effective strategy as proved by many examples in the literature to overcome the main drawbacks of the TiO₂ photocata-

lyst. Hence continued research with new dopants and doping strategies will be observed in near future.

Although there is an increased interest in the use of doped titanium oxide for photocatalytic degradation of various pollutants, the research is far from developing a cost effective and highly efficient water purification technology. The challenges and future directions of research will be:

- The development of highly efficient doped TiO₂ nanomaterial that can be easily prepared and scaled up;
- The development of a suitable material to completely degrade the pollutants in minimum time and maximum efficiency;
- The development of a suitable photocatalytic material that can operate at simple working conditions and that do not need special requirements such as UV irradiation OR high temperatures etc;
- It will be ideal to find a material with suitable doping that can degrade most of the types of dyes used in industries from their mixture. This is because most

Table 2. Important latest reports about doped TiO₂ for dye degradation application

Material or Dopant/s	Dye used	Main observation/s results	Citation
Bi-doped TiO ₂ supported on powdered activated carbon (Bi ₂ O ₃ /TiO ₂ /PAC)	MO	The material exhibits 71.2% photocatalytic efficiency under visible light irradiation for 1 hr with an intensity of 750 W/m ² and at pH 7	[92]
TiO ₂ nanorod arrays decorated by nitrogen-doped carbon TNR@CN-C ₃ N ₄ /FTO	MO	Ternary TNR@CN-C ₃ N ₄ /FTO photoelectrode indicated the highest photocurrent density (0.45 mA/cm ² at 0.6 V) and the best PEC degradation rate 94.2% at 1.5 V of methyl orange	[93]
Fe-doped TiO ₂	AO ₇	The Fe doping showed enhanced photocatalytic activity of TiO ₂ for AO ₇ degradation, due to the increase in surface area, the facilitated charge transfer via Fe-dopant, and a red shift of absorbable wavelength. Fe-doped TiO ₂ under UV irradiation for 6 h shows 50% efficiency for AO ₇ degradation.	[94]
Active nitrogen doped titania (N/TiO ₂)	MB	The mesoporous N/TiO ₂ (1:1 N/Ti, 42% A, 58% R with 2.91 eV band gap energy) demonstrated 97% photodegradation activity along with a highest photodegradation rate of 0.033 min ⁻¹ , which was 17 times faster than the undoped TiO ₂ .	[95]
Titanium dioxide nanoparticles dual doped with zinc and manganese	Rh B	The 100% degradation of dye was achieved at optimum condition of 1 mol %-Zn and 2 mol %-Mn molar ratios. The highest photodegradation rate constant was 0.0238 min ⁻¹	[96]
Pristine and chromium (Cr) metal ion-doped titanium dioxide nanoparticles [Cr(x)TiO ₂ (1 - x)]	Malachite green	The pristine TiO ₂ showed better photocatalytic activity as compared to Cr-doped TiO ₂ irrespective of the Cr concentration. The degradation efficiency of Cr-doped (10%) TiO ₂ is reduced by 10% compared to bare TiO ₂ .	[97]
Mesoporous N-doped TiO ₂ /Si-O-C-N ceramic nanocomposites	MB	The mesoporous N-doped TiO ₂ nanocomposite manifested high adsorption capacity and visible light photocatalytic activity for degradation of methylene blue. The doping reduces the band gap, thereby harness more light in the visible light wavelength regime. The hydroxyl radicals and the superoxide anions formed degrade the dye	[98]
Boron Doped TiO ₂	Rh B	B-TiO ₂ showed high photocatalytic degradation ability toward organic dye of rhodamine B under visible light irradiation.	[99]
N-doped TiO ₂	MO	The N-TiO ₂ /ASep(N ₂)/PMS system degraded about 95% of the methyl orange within 60 min.	[100]
Mixed phased titania co-doped Sm ³⁺ /Er ³⁺ composites	Acid Blue 113	The UV-Vis-DRS analysis showed an energy band gap value of 3.26, 3.02, and 2.80 eV, for un-doped, (3.0 mol %) Sm ³⁺ doped, and (0.6 mol %) Er ³⁺ /(3.0 mol %) Sm ³⁺ codoped TiO ₂ monoliths. The model organic dye pollutant dissipated within 30 min of visible light irradiation	[101]
Au-modified N, S-doped TiO ₂ nanoparticles	MB	In this work, plasmonic photocatalyst has been developed by a clay-supported anisotropic Au nanoparticle-deposited N, S-doped TiO ₂ . It showed a 9-fold increase in the degradation rate constant and the complete degradation of MB was done under sunlight after 5 h in the presence of an electrolyte (Na ₂ HPO ₄).	[102]
Dy-doped TiO ₂ nanoparticles	MB	Heterogeneous nanostructured Dy-doped TiO ₂ nanoparticles hybrid with Monoclinic TiO ₂ nanobelts (Dy/TNBs) was fabricated via hydrothermal method. Enhanced photocatalytic activity under both UV and fluorescence irradiation was found on Dy/TNB samples. Complete degradation of the dye was achieved in 120 min.	[103]

Table 2. (Contd.)

Material or Dopant/s	Dye used	Main observation/s results	Citation
Nitrogen-doped carbon enhanced mesoporous TiO ₂	MO	N-doped carbon (NC) and mesoporous TiO ₂ (mTiO ₂) interpenetrating hetero-structured nanospheres revealed the photodegradation efficiency of methyl orange was up to 97.7%.	[104]
N and Ag doped and co-doped TiO ₂	MB	Single and co-doped TiO ₂ with nitrogen and silver were prepared by in-situ solvothermal methods. The N doping significantly enhanced homogenous surface morphology and specific surface area of the photocatalyst and Ag doping was narrowed the band gap energy. The highest photocatalytic activity and recyclability were reached in 5% N/Ag–TiO ₂ showed the efficiency of 98.82% for methylene blue (MB) dye degradation and 37.5% for NH ₃ removal in 6 h.	[105]
Dye doped TiO ₂ nanocomposite	MB	One-pot in situ synthesis of titanium nano-particles were carried out in the presence of N719 dye. The dye doped TiO ₂ showed exceptional dye degradation efficiency as in 25 min, 99% of methylene blue was degraded.	[106]
Fe ³⁺ -doped TiO ₂	RhB	At 3.0 bar inlet pressure for 10 mg/L initial conc. of RhB solution at 40°C in the presence of Fe ³⁺ -doped TiO ₂ with 0.05:1.00 M ratio of Fe and Ti, the best hydrodynamic cavitations degradation ratio obtained was 91.11%.	[57]
Ti ³⁺ self-doped rutile/anatase/TiO ₂ (B) mixed-crystal tri-phase heterojunctions	MO	The photocatalyst consisted anatase/rutile TiO ₂ nanoparticles and 1D TiO ₂ (B) single-crystalline nanorods, which formed rutile/anatase/TiO ₂ (B) tri-phase heterojunctions. The visible-light-driven photocatalytic degradation rates of methyl orange and phenol observed were ~98 and 97%, which are 2.2 and 1.8 times higher than that of commercial Degussa P25, 2.3 and 2.2 times higher than that of pure TiO ₂ .	[107]
Nitrogen-doped carbon quantum dots/TiO ₂ composites (N-CDs/TiO ₂)	Rh B	The degradation testing of rhodamine B under visible-light irradiation ($\lambda \geq 400$ nm) shows that the photocatalytic performance of N-CDs/TiO _{2-x} substantially improved relative to pure TiO ₂ . The optimal photocatalytic performance of N-CDs/TiO ₂₋₁ totally removed the RhB in 120 min, which is 11.42 times over that of TiO ₂ .	[108]
Rhodium/Antimony co-doped TiO ₂ nanorod and titanate nanotube (RS-TONR/ TNT)	Orange (II)	Synergistic removal and degradation was tested in this study with various heavy metals, Orange (II) dye, and Bisphenol A. The adsorbed metals were found to enhance the photocatalytic degradation of the organic pollutants; Cu was most effective, with degradation exceeding 70% for the dye and 80% for Bisphenol A after 5 h of treatment.	[109]
Europium Doped TiO ₂ –Ta ₂ O ₅ Heterostructure	Indigo carmine	In this work, europium doped TiO ₂ –Ta ₂ O ₅ mixed oxide heterostructure was prepared by wet impregnation method. Europium doping in TiO ₂ and corresponding 0.5 Eu 90%–TiTa composite showed improved visible light absorption and enhanced photoactivity. It showed 90% degradation of the dye in 30 min and with the highest rate constant 0.073 /min	[110]
Ce and Mn doped TiO ₂ coated carbon nanospheres (CNS)	Acid Yellow 29 (AY-29) and Acid Green 25 (AG-25)	The results obtained showed that the doped TiO ₂ are efficient for degradation of dyes under visible light as compared to bare TiO ₂ . The doped TiO ₂ 3.0% (Ce) and 1.5% (Mn) showed the highest photocatalytic efficiency.	[30]

Table 2. (Contd.)

Material or Dopant/s	Dye used	Main observation/s results	Citation
L-cysteine doped TiO ₂ /CdS	MO, MB and Rh B	Photocatalytic activity of the nanocomposites (pure TiO ₂ , L-cysteine doped TiO ₂ and L-cysteine doped TiO ₂ /CdS) was evaluated during degradation of methyl orange (MO), methylene blue (MB) and rhodamine B (RB) as azo dyes. As a result, L-cysteine (2%) doped TiO ₂ /CdS (10%) was completely removed 10 mg of MO, MB and RB under visible light irradiation after 210, 200 and 180 min, respectively.	[111]
TiO ₂ nanoparticle-doped Ag (Ag/TNPs)	MO	This study reports the negative effect of effluent organic matter (EfOM) on photocatalytic activity of the photocatalyst. It revealed a nonsynergistic effect between nanomaterial and EfOM for photocatalysis. EfOM would have a negative effect on photocatalytic degradation of organic compounds by Ag/TNPs in the aquatic environment.	[112]
N-doped TiO ₂ and TiO ₂ -CoS Nanostructures	Rh B	The N-doped TiO ₂ nanofibrous (NTNF)-CoS nanocomposite showed superior photocatalytic degradation of RhB under visible light. The NTNF-CoS nano-composite showed highest photocatalytic activity among all photocatalysts. The composite degraded about 80% RhB in 60 min.	[113]
Ni-doped and Ni/Cr co-doped TiO ₂ nanotubes	MB	The un-doped, doped and co-doped TiO ₂ nanoparticles, the 6Ni/4Cr co-doped TiO ₂ sample exhibited an efficiency of 95.6% and excellent stability towards the photocatalytic degradation of the dye.	[114]
Gd-doped TiO ₂ nanoparticles	MB	The results showed that the doping with Gd could reduce the radiative recombination process of photogenerated electron-hole pairs in TiO ₂ and induce a significant enhancement in photocatalytic activity. The photocatalytic degradation rate of MB was found to be improved when Gadolinium dopant be in the 0.1–1 mol % ranges. In particular, 0.1 mol % Gd-TiO ₂ nano-particles showed the best photocatalytic activity with a reduction of 80% of MB concentration after 6 h of irradiation.	[115]
Eu ³⁺ doped TiO ₂ -carbon core-shell nanohybrids	MB (2-CP)	This work reports sustainable synthesis of Eu ³⁺ doped TiO ₂ -carbon core-shell nanohybrids (0.5–2.0 mol % Eu ³⁺) using a simple green-chili-based biogenic method. 1.5 mol % Eu ³⁺ doped core shell nanohybrid, annealed at 600 °C exhibits highest removal efficiency 91.5 and 76.8% for MB and 2-CP respectively. The Eu ³⁺ proved to boost the photocatalytic performance.	[116]
N doped TiO ₂ -SiO ₂	MB	Photo degradation of toluene gas and methylene blue (MB) dye under UV light confirmed that the sample heat treated at 450°C shows a high photocatalytic activity. The sample calcined at 450°C decomposes MB dye up to 95% within 5 h while the the sample calcined at 180°C decompose 65% of the dye.	[117]
Fibrous Sm ³⁺ -Doped Titanium Dioxide	MO	This work, Fibrous Sm ³⁺ -doped TiO ₂ (Sm/TiO ₂) were synthesized using collagen fibers as a template. The highest photocatalytic activity was shown with a dopant amount of 4% samarium calcined at 600°C, and the degradation rate of methyl orange reaches 98.22% after 40 min using metal halide lamp (350 W) as illuminant.	[118]
Mn ²⁺ -Ni ²⁺ Co-doped nanotitania	Allura red (AR)	The results revealed that AR degrades in 60 minutes at doping concentrations 0.25 wt % of Mn ²⁺ ion and 1.0 wt % of Ni ²⁺ ion in TiO ₂ (NMT2) at pH 4, catalyst dose 0.070 g/L and at AR initial dye concentration 0.010 g/L.	[119]

Table 2. (Contd.)

Material or Dopant/s	Dye used	Main observation/s results	Citation
Ag, Sn or Zn doped TiO ₂ thin films	MB, MO	In this work, nanocrystalline anatase TiO ₂ thin films doped with silver (Ag), tin (Sn) or zinc (Zn) with up to 5 mole percent were prepared. The photocatalytic degradation of methylene blue and methyl orange was achieved. The films showed pseudo first-order kinetics. The apparent rate constant values were $4.30 \times 10^{-3}/S$ for MB and $5.34 \times 10^{-3}/S$ for MO)	[120]
Gd ³⁺ doped TiO ₂ and Gd ₂ O ₃ modified TiO ₂ prepared via ball milling	MB, Rh B	Gd ³⁺ /TiO ₂ and Gd ₂ O ₃ /TiO ₂ nanoparticles were prepared by ball milling, degraded MB (25 mg/L) with degradation reaction rate constants of 0.0713 and 0.0588 min ⁻¹ respectively. The degradation rates of RB (30 mg/L) in 60 min were 97.9, 90.1% for Gd ³⁺ /TiO ₂ (2.5 mol %) and Gd ₂ O ₃ /TiO ₂ (0.5 mol %) respectively.	[121]
Rutile-Anatase Fe-doped TiO ₂	Azucryl red	Excellent photocatalytic degradation of azucryl red was achieved by 0.2% Fe doped TiO ₂ sample. The complete degradation (100%) of the dye was achieved within only 10 min.	[122]

of the studies have been concentrated on degradation of one or two dyes only;

—The development of a photocatalyst that can be repeatedly used (recyclability) for several cycles of the degradation of the pollutants;

—Cost aspect of the material is also going to be a crucial point because although doping with some fancy materials such as rare earth may increase the photocatalytic activity but the cost of these materials are very high.

Therefore, although very intense research has been carried out on TiO₂ and doped TiO₂ based photocatalysts for dye degradation all above challenges still exists. Hence, the research will continue until a suitable material will be invented to develop a water purification technology based on it.

ACKNOWLEDGMENTS

The authors gratefully acknowledge the financial support received from Chhatrapati Shahu Maharaj Research Training and Human Development Institute (SARTHI), Pune (Government of Maharashtra) for the Chhatrapati Shahu Maharaj Senior Research Fellowship-(CMSRF) 2019, DST PURSE Phase-II (2018–2022) and UGC DSA Phase-II (2018–2023).

CONFLICT OF INTEREST

The authors declare that they have no conflicts of interest.

REFERENCES

1. S. Gunti, A. Kumar, and M. K. Ram, *Int. Mater. Rev.* **63**, 257 (2017).
<https://doi.org/10.1080/09506608.2017.1379264>
2. S. Ghasemi, S. Rahimnejad, S. R. Setayesh, et al., *J. Hazard. Mater.* **172**, 1573 (2009).
<https://doi.org/10.1016/j.jhazmat.2009.08.029>
3. A. Ajmal, I. Majeed, R. N. Malik, et al., *RSC Adv.* **4**, 37003 (2014).
<https://doi.org/10.1039/C4RA06658H>
4. S. S. Shinde, C. H. Bhosale, and K. Y. Rajpure, *J. Photochem. Photobiol. B* **103**, 111 (2011).
<https://doi.org/10.1016/j.jphotobiol.2011.02.002>
5. M. A. Mahadik, S. S. Shinde, H. M. Pathan, et al., *J. Photochem. Photobiol. B* **141**, 315 (2014).
<https://doi.org/10.1016/j.jphotobiol.2014.10.014>
6. S. S. Shinde, P. S. Shinde, C. H. Bhosale, et al., *J. Photochem. Photobiol. B* **104**, 425 (2011).
<https://doi.org/10.1016/j.jphotobiol.2011.04.010>
7. C. N. C. Hitam and A. A. Jalil, *J. Environ. Manage.* **258**, 110050 (2020).
<https://doi.org/10.1016/j.jenvman.2019.110050>
8. T. Ochiai and A. Fujishima, *J. Photochem. Photobiol. C* **13**, 247 (2012).
<https://doi.org/10.1016/j.jphotochemrev.2012.07.001>
9. W. H. Glaze, J.-W. Kang, and D. H. Chapin, *Ozone Sci. Eng.* **9**, 335 (1987).
<https://doi.org/10.1080/01919518708552148>
10. C. Yang, W. Dong, G. Cui, et al., *RSC Adv.* **7**, 23699 (2017).
<https://doi.org/10.1039/C7RA02423A>
11. M. Tasbihi, I. Calin, and A. Suligoj, *J. Photochem. Photobiol. Chem.* **336**, 89 (2017).
<https://doi.org/10.1016/j.jphotochem.2016.12.025>
12. W.-R. Tang, T. Wu, and Y.-W. Lin, *Micro Nano Lett.* **14**, 359 (2019).
<https://doi.org/10.1049/mnl.2018.5562>
13. Y. Mahmiani, A. M. Sevim, and A. Gul, *J. Photochem. Photobiol. Chem.* **321**, 24 (2016).
<https://doi.org/10.1016/j.jphotochem.2015.12.015>

14. S. S. Shinde, C. H. Bhosale, and K. Y. Rajpure, *J. Mol. Catal. Chem.* **347**, 65 (2011).
<https://doi.org/10.1016/j.molcata.2011.07.012>
15. H. Huang, B. Pradhan, J. Hofkens, et al., *ACS Energy Lett.* **5**, 1107 (2020).
<https://doi.org/10.1021/acsenerylett.0c00058>
16. Y. Li and S. C. E. Tsang, *Mater. Today Sustain.* **9**, 100032 (2020).
<https://doi.org/10.1016/j.mtsust.2020.100032>
17. S. W. Verbruggen, *J. Photochem. Photobiol. C* **24**, 64 (2015).
<https://doi.org/10.1016/j.jphotochemrev.2015.07.001>
18. X. Kang, S. Liu, Z. Dai, et al., *Catalysts* **9**, 191 (2019).
<https://doi.org/10.3390/catal9020191>
19. S. Ghasemi, S. R. Setayesh, A. Habibi-Yangjeh, et al., *J. Hazard. Mater.* **199–200**, 170 (2012).
<https://doi.org/10.1016/j.jhazmat.2011.10.080>
20. H. Park, H. Kim, G. Moon, and W. Choi, *Energy Environ. Sci.* **9**, 411 (2016).
<https://doi.org/10.1039/C5EE02575C>
21. R. Daghrir, P. Drogui, and D. Robert, *Ind. Eng. Chem. Res.* **52**, 3581 (2013).
<https://doi.org/10.1021/ie303468t>
22. A. G. Tamirat, J. Rick, A. A. Dubale, et al., *Nanoscale Horiz.* **1**, 243 (2016).
<https://doi.org/10.1039/C5NH00098J>
23. A. Fujishima and K. Honda, *Nature (London, U.K.)* **238** (5358), 37 (1972).
<https://doi.org/10.1038/238037a0>
24. S. G. Kumar and L. G. Devi, *J. Phys. Chem. A* **115**, 13211 (2011).
<https://doi.org/10.1021/jp204364a>
25. P. Yadav, P. K. Dwivedi, S. Tonda, et al., in *Green Photocatalysts*, Ed. by Mu. Naushad, S. Rajendran, and E. Lichtfouse, Vol. 34 of *Environmental Chemistry for a Sustainable World* (Springer Int., Cham, 2020), p. 89.
26. D. Li, H. Song, X. Meng, et al., *Nanomaterials* **10**, 546 (2020).
<https://doi.org/10.3390/nano10030546>
27. V. Etacheri, C. di Valentin, J. Schneider, et al., *J. Photochem. Photobiol. C* **25**, 1 (2015).
<https://doi.org/10.1016/j.jphotochemrev.2015.08.003>
28. V. Krishna, W. Bai, Z. Han, et al., *Sci. Rep.* **8**, 1894 (2018).
<https://doi.org/10.1038/s41598-018-19972-0>
29. F. Huang, A. Yan, and H. Zhao, in *Semiconductor Photocatalysis—Materials, Mechanisms and Applications*, Ed. by W. Cao (InTech, Rijeka, Croatia, 2016).
30. W. Raza, M. M. Haque, M. Muneer, and D. Bahnemann, *Arab. J. Chem.* **12**, 3534 (2019).
<https://doi.org/10.1016/j.arabjc.2015.09.002>
31. Z. Li and X. Meng, *J. Alloys Compd.* **830**, 154669 (2020).
<https://doi.org/10.1016/j.jallcom.2020.154669>
32. A. Juma, I. Oja Acik, A. T. Oluwabi, et al., *Appl. Surf. Sci.* **387**, 539 (2016).
<https://doi.org/10.1016/j.apsusc.2016.06.093>
33. C. H. A. Tsang, K. Li, Y. Zeng, et al., *Environ. Int.* **125**, 200 (2019).
<https://doi.org/10.1016/j.envint.2019.01.015>
34. S. H. Mohamed, M. El-Hagary, and S. Althoyaib, *Appl. Phys. A* **111**, 1207 (2013).
<https://doi.org/10.1007/s00339-012-7367-7>
35. L. Santamaria, M. A. Vicente, S. A. Korili and A. Gil, *Environ. Technol.* **41**, 2073 (2020).
<https://doi.org/10.1080/09593330.2018.1555285>
36. B. Gomathi Thanga Keerthana, T. Solaiyammal, S. Muniyappan, and P. Murugakoothan, *Mater. Lett.* **220**, 20 (2018).
<https://doi.org/10.1016/j.matlet.2018.02.119>
37. S. V. Mohite, V. V. Ganbavle, and K. Y. Rajpure, *Mater. Res. Bull.* **95**, 491 (2017).
<https://doi.org/10.1016/j.materresbull.2017.06.043>
38. O. Ola and M. M. Maroto-Valer, *J. Photochem. Photobiol. C* **24**, 16 (2015).
<https://doi.org/10.1016/j.jphotochemrev.2015.06.001>
39. Q. Guo, C. Zhou, Z. Ma, and X. Yang, *Adv. Mater.* **31**, 1901997 (2019).
<https://doi.org/10.1002/adma.201901997>
40. A. Pimentel, D. Nunes, S. Pereira, et al., in *Semiconductor Photocatalysis*, Ed. by W. Cao (InTech, Rijeka, Croatia, 2016).
<https://doi.org/10.5772/63237>
41. U. Diebold, N. Ruzycski, G. S. Herman, and A. Selloni, *Catal. Today* **85** (2–4), 93 (2003).
[https://doi.org/10.1016/S0920-5861\(03\)00378-X](https://doi.org/10.1016/S0920-5861(03)00378-X)
42. R. Asahi, Y. Taga, W. Mannstadt, and A. J. Freeman, *Phys. Rev. B* **61**, 7459 (2000).
<https://doi.org/10.1103/PhysRevB.61.7459>
43. A. A. Umar, S. K. Md Saad, M. I. Ali Umar, et al., *Opt. Mater.* **75**, 390 (2018).
<https://doi.org/10.1016/j.optmat.2017.10.002>
44. J. Zhang, P. Zhou, J. Liu, and J. Yu, *Phys. Chem. Chem. Phys.* **16**, 20382 (2014).
<https://doi.org/10.1039/C4CP02201G>
45. J. Schneider, M. Matsuoka, M. Takeuchi, et al., *Chem. Rev.* **114**, 9919 (2014).
<https://doi.org/10.1021/cr5001892>
46. J. C. Contreras-Ruiz, S. Martínez-Gallegos, E. Ordoñez, et al., *J. Electron. Mater.* **46**, 1658 (2017).
<https://doi.org/10.1007/s11664-016-5209-7>
47. M. Pelaez, N. T. Nolan, S. C. Pillai, et al., *Appl. Catal. B* **125**, 331 (2012).
<https://doi.org/10.1016/j.apcatb.2012.05.036>
48. A. Hajjaji, K. Trabelsi, A. Atyaoui, et al., *Nanoscale Res. Lett.* **9**, 543 (2014).
<https://doi.org/10.1186/1556-276X-9-543>
49. J. Low, B. Cheng, and J. Yu, *Appl. Surf. Sci.* **392**, 658 (2017).
<https://doi.org/10.1016/j.apsusc.2016.09.093>
50. E. Üzer, P. Kumar, R. Kisslinger, et al., *ACS Appl. Nano Mater.* **2**, 3358 (2019).
<https://doi.org/10.1021/acsnm.9b00221>
51. V. Štengl, S. Bakardjieva, and N. Murafa, *Mater. Chem. Phys.* **114**, 217 (2009).
<https://doi.org/10.1016/j.matchemphys.2008.09.025>
52. Z. Zhang, Q. Wu, G. Johnson, et al., *J. Am. Chem. Soc.* **141**, 16548 (2019).
<https://doi.org/10.1021/jacs.9b06389>

53. Q. Wang, T. Hisatomi, S. S. K. Ma, et al., *Chem. Mater.* **26**, 4144 (2014).
<https://doi.org/10.1021/cm5011983>
54. S. G. Ullattil and R. M. Ramakrishnan, *ACS Appl. Nano Mater.* **1**, 4045 (2018).
<https://doi.org/10.1021/acsnm.8b00824>
55. C. Ly, X. Lan, L. Wang, et al., *Catal. Sci. Technol.* **9**, 6124 (2019).
<https://doi.org/10.1039/C9CY01687B>
56. H. Rajput, R. Changotra, V. K. Sangal, et al., *Chemosphere* **218**, 687 (2019).
<https://doi.org/10.1016/j.chemosphere.2018.11.157>
57. G. Li, L. Yi, J. Wang, and Y. Song, *Ultrason. Sonochem.* **60**, 104806 (2020).
<https://doi.org/10.1016/j.ultsonch.2019.104806>
58. W. Fang, F. Dappozze, C. Guillard, et al., *J. Phys. Chem. C* **121**, 17068 (2017).
<https://doi.org/10.1021/acs.jpcc.7b03724>
59. H. Qiu, X. Ma, C. Sun, et al., *Appl. Surf. Sci.* **506**, 145021 (2020).
<https://doi.org/10.1016/j.apsusc.2019.145021>
60. T. S. Natarajan, K. Natarajan, H. C. Bajaj, and R. J. Tayade, *J. Nanopart. Res.* **15**, 1669 (2013).
<https://doi.org/10.1007/s11051-013-1669-3>
61. H. Li, D. Wang, P. Wang, et al., *Chem.-Eur. J.* **15**, 12521 (2009).
<https://doi.org/10.1002/chem.200901193>
62. M. Hinojosa-Reyes, R. Camposeco-Solis, F. Ruiz, et al., *Mater. Sci. Semicond. Process* **100**, 130 (2019).
<https://doi.org/10.1016/j.mssp.2019.04.050>
63. S. Cao, S. Zhang, T. Zhang, et al., *J. Mater. Chem. C* **6**, 4007 (2018).
<https://doi.org/10.1039/C8TC00185E>
64. S. P. Takle, S. D. Naik, S. K. Khore, et al., *RSC Adv.* **8**, 20394 (2018).
<https://doi.org/10.1039/C8RA02869A>
65. Y. Qiao, S. Li, W. Liu, et al., *Nanomaterials* **8**, 43 (2018).
<https://doi.org/10.3390/nano8010043>
66. M. Pawar, S. Topcu Sengođular, and P. Gouma, *J. Nanomater.*, 1–13 (2018).
<https://doi.org/10.1155/2018/5953609>
67. M. Reli, N. Ambrožová, M. Šihor, et al., *Appl. Catal. B* **178**, 108 (2015).
<https://doi.org/10.1016/j.apcatb.2014.10.021>
68. H. Phattepur, B. S. Gowrishankar, and G. Nagaraju, *Indian Chem. Eng.* **61**, 167 (2019).
<https://doi.org/10.1080/00194506.2018.1529632>
69. J. Choi, P. Sudhagar, P. Lakshmipathiraj, et al., *RSC Adv.* **4**, 11750 (2014).
<https://doi.org/10.1039/C3RA46851H>
70. R. Bashiri, N. M. Mohamed, C. F. Kait, et al., *J. Environ. Chem. Eng.* **5**, 3207 (2017).
<https://doi.org/10.1016/j.jece.2017.06.027>
71. P. Sanitnon, S. Chiarakorn, C. Chawengkijwanich, et al., *J. Aust. Ceram. Soc.* **56**, 579 (2020).
<https://doi.org/10.1007/s41779-019-00368-w>
72. T. Ly, J. Zhao, M. Chen, et al., *Materials* **11**, 1946 (2018).
<https://doi.org/10.3390/ma11101946>
73. T. Iihoshi, T. Ohwaki, J. J. M. Vequizo, et al., *Appl. Catal. B* **248**, 249 (2019).
<https://doi.org/10.1016/j.apcatb.2019.01.046>
74. H. Zhang, Z. Xing, Y. Zhang, et al., *RSC Adv.* **5**, 107150 (2015).
<https://doi.org/10.1039/C5RA23743B>
75. W. S. A. El-Yazeed and A. I. Ahmed, *Inorg. Chem. Commun.* **105**, 102 (2019).
<https://doi.org/10.1016/j.inoche.2019.04.034>
76. X. Liu, L. Cao, W. Sun, et al., *Res. Chem. Intermed.* **42**, 6289 (2016).
<https://doi.org/10.1007/s11164-016-2461-7>
77. Md. A. Hossain, Md. Elias, and D. R. Sarker, *Res. Chem. Intermed.* **44**, 2667 (2018).
<https://doi.org/10.1007/s11164-018-3253-z>
78. Z. Li, F. Cao, L. Wang, et al., *New J. Chem.* **44**, 537 (2020).
<https://doi.org/10.1039/C9NJ04107A>
79. M. Dahl, Y. Liu, and Y. Yin, *Chem. Rev.* **114**, 9853 (2014).
<https://doi.org/10.1021/cr400634p>
80. C. Zhan, F. Chen, J. Yang, et al., *J. Hazard. Mater.* **267**, 88 (2014).
<https://doi.org/10.1016/j.jhazmat.2013.12.038>
81. K. Vasu, M. B. Sreedhara, J. Ghatak, and C. N. R. Rao, *ACS Appl. Mater. Interfaces* **8**, 7897 (2016).
<https://doi.org/10.1021/acsami.6b00628>
82. Y. Xiong, D. He, R. Jaber, et al., *J. Phys. Chem. C* **121**, 9929 (2017).
<https://doi.org/10.1021/acs.jpcc.7b01615>
83. F. Wang, F. Li, L. Zhang, et al., *Mater. Res. Bull.* **87**, 20 (2017).
<https://doi.org/10.1016/j.materresbull.2016.11.014>
84. G. Hosseinzadeh, H. Rasoulnezhad, N. Ghasemian, and R. Hosseinzadeh, *J. Aust. Ceram. Soc.* **55**, 387 (2019).
<https://doi.org/10.1007/s41779-018-0246-8>
85. H. Rasoulnezhad, G. Hosseinzadeh, R. Hosseinzadeh, and N. Ghasemian, *J. Adv. Ceram.* **7**, 185 (2018).
<https://doi.org/10.1007/s40145-018-0270-8>
86. E. M. Samsudin, S. B. Abd Hamid, J. C. Juan, et al., *RSC Adv.* **5**, 44041 (2015).
<https://doi.org/10.1039/C5RA00890E>
87. S. Cho, C. Ahn, J. Park, and S. Jeon, *Nanoscale* **10**, 9747 (2018).
<https://doi.org/10.1039/C8NR02330A>
88. E. L. Castellanos-Leal, P. Acevedo-Peña, V. R. Güiiza-Argüello, and E. M. Córdoba-Tuta, *Mater. Res.* **20**, 487 (2017).
<https://doi.org/10.1590/1980-5373-mr-2016-0214>
89. E. M. Bayan, T. G. Lupeiko, L. E. Pustovaya, et al., *J. Alloys Compd.* **822**, 153662 (2020).
<https://doi.org/10.1016/j.jallcom.2020.153662>
90. H. Kmentová, D. Nandan, Š. Kment, et al., *Catal. Today* **328**, 111 (2019).
<https://doi.org/10.1016/j.cattod.2019.01.024>
91. R. Wang, K. Shi, D. Huang, et al., *Sci. Rep.* **9**, 18744 (2019).
<https://doi.org/10.1038/s41598-019-54320-w>

92. Y. Shang, X. Li, Y. Yang, et al., *J. Environ. Sci.* **94**, 40 (2020).
<https://doi.org/10.1016/j.jes.2020.03.044>
93. K. Huang, C. Li, X. Zhang, et al., *Appl. Surf. Sci.* **518**, 146219 (2020).
<https://doi.org/10.1016/j.apsusc.2020.146219>
94. J.-H. Shen, H.-Y. Chuang, Z.-W. Jiang, et al., *Chemosphere* **251**, 126380 (2020).
<https://doi.org/10.1016/j.chemosphere.2020.126380>
95. E. Assayehegn, A. Solaiappan, Y. Chebude, and E. Alemayehu, *Appl. Surf. Sci.* **515**, 145966 (2020).
<https://doi.org/10.1016/j.apsusc.2020.145966>
96. C. Wattanawikkam and W. Pecharapa, *Radiat. Phys. Chem.* **171**, 108714 (2020).
<https://doi.org/10.1016/j.radphyschem.2020.108714>
97. J. Bansal, R. Tabassum, S. K. Swami, et al., *Appl. Phys. A* **126**, 363 (2020).
<https://doi.org/10.1007/s00339-020-03536-z>
98. E. Wasan Awin, A. Lale, K. C. Hari Kumar, et al., *Materials* **11**, 362 (2018).
<https://doi.org/10.3390/ma11030362>
99. P. Niu, G. Wu, P. Chen, et al., *Front. Chem.* **8**, 172 (2020).
<https://doi.org/10.3389/fchem.2020.00172>
100. Q. Wang, Y. Cui, R. Huang, et al., *Chem. Eng. J.* **383**, 123142 (2020).
<https://doi.org/10.1016/j.cej.2019.123142>
101. N. K. Sompalli, A. Das, S. Syamal De, et al., *Appl. Surf. Sci.* **504**, 144350 (2019).
<https://doi.org/10.1016/j.apsusc.2019.144350>
102. C. Hu, T.-R. Su, T.-J. Lin, et al., *New J. Chem.* **42**, 3999 (2018).
<https://doi.org/10.1039/C7NJ03337K>
103. T. S. Nwe, L. Sikong, R. Kokoo, and M. Khangkhamano, *Curr. Appl. Phys.* **20**, 249 (2020).
<https://doi.org/10.1016/j.cap.2019.11.008>
104. D. Li, Y. Liu, H. Liu, et al., *Res. Chem. Intermed.* **46**, 1065 (2020).
<https://doi.org/10.1007/s11164-018-3531-9>
105. A. Sirivallop, T. Areerob, and S. Chiarakorn, *Catalysts* **10**, 251 (2020).
<https://doi.org/10.3390/catal10020251>
106. I. Herath, I. Perera, and C. Hettiarachchi, *Pigment Resin Technol.* **49**, 1 (2020).
<https://doi.org/10.1108/PRT-03-2019-0031>
107. J. Kuang, Z. Xing, and J. Yin, *Arab. J. Chem.* **13**, 2568 (2020).
<https://doi.org/10.1016/j.arabjc.2018.06.010>
108. R. Wang, X. Ma, K. Hao et al., *Mater. Res. Express* **7**, 025022 (2020).
<https://doi.org/10.1088/2053-1591/ab71cf>
109. L. K. Dhandole, S.-G. Kim, H.-S. Bae, et al., *Environ. Res.* **180**, 108651 (2020).
<https://doi.org/10.1016/j.envres.2019.108651>
110. S. G. Ghugal, D. Vidyasagar, and S. G. Ghugal, *Chem. Sel.* **5**, 2981 (2020).
<https://doi.org/10.1002/slct.201904150>
111. W. Raza, M. M. Haque, M. Muneer, and D. Bahnemann, *Arab. J. Chem.* **12**, 3534 (2015).
<https://doi.org/10.1016/j.arabjc.2015.09.002>
112. H. Deng, H. He, S. Sun, and X. Zhu, *Environ. Sci. Pollut. Res.* **26**, 35900 (2019).
<https://doi.org/10.1007/s11356-019-06728-0>
113. K. Dey, S. Ganguli, and M. S. Alam, *Chem. Sel.* **4**, 12464 (2019).
<https://doi.org/10.1002/slct.201903406>
114. M. Shaban, A. M. Ahmed, N. Shehata, et al., *J. Colloid Interface Sci.* **555**, 31 (2019).
<https://doi.org/10.1016/j.jcis.2019.07.070>
115. M. Ben Chobba, M. Messaoud, M. L. Weththimuni, et al., *Environ. Sci. Pollut. Res.* **26**, 32734 (2019).
<https://doi.org/10.1007/s11356-019-04680-7>
116. P. V. Rajeswari, S. Ram, and D. Pradhan, *Appl. Surf. Sci.* **492**, 473 (2019).
<https://doi.org/10.1016/j.apsusc.2019.06.169>
117. V. B. Koli, S. Mavengere, and J.-S. Kim, *Appl. Surf. Sci.* **491**, 60 (2019).
<https://doi.org/10.1016/j.apsusc.2019.06.123>
118. Li-Yuan Zhang, X.-J. Wan, and Y.-H. You, *Russ. J. Phys. Chem. A* **93**, 2087 (2019).
<https://doi.org/10.1134/S0036024419100340>
119. S. R. Mditana, S. R. Tirukkovalluri, S. A. Alim, and I. M. Raju, *Int. J. Innov. Technol. Explor. Eng.* **8**, 2278 (2019).
<https://doi.org/10.35940/ijitee.K2458.1081219>
120. M. K. Tariq, A. Riaz, R. Khan, et al., *Mater. Res. Express* **6**, 106435 (2019).
<https://doi.org/10.1088/2053-1591/ab3efd>
121. D. Wu, C. Li, D. Zhang, et al., *J. Rare Earths* **37**, 845 (2019).
<https://doi.org/10.1016/j.jre.2018.10.011>
122. A. Kerrami, L. Mahtout, F. Bensouici, et al., *Mater. Res. Express* **6** (2019).
<https://doi.org/10.1088/2053-1591/ab2677>

SPELL: OK